

Article

Battery Management for Improved Performance in Hybrid Electric Vehicles

Carlos Armenta-Déu 

Facultad de Ciencias Físicas, Universidad Complutense de Madrid, 28040 Madrid, Spain; cardeu@fis.ucm.es

Abstract: This study aims to improve the battery performance in hybrid electric vehicles (HEVs) by reducing the vehicle speed. We developed a specific protocol for managing battery use and optimizing the energy consumption rate to achieve this goal. The protocol automatically controls the driving operation, avoiding incompatible driving patterns with an energy-saving mode and performance improvement. This protocol was applied to a simulation process to predict energy rate lowering and battery performance enhancement. The proposed protocol applies to any hybrid electric vehicle type and any route conditions since it uses vehicle mass, drag and rolling coefficients, and road slope as variable parameters to determine the minimum energy consumption rate. We performed experimental tests to validate the simulation data and the proposed protocol. Furthermore, the protocol applies to variable starting vehicle speeds, from 10 to 50 km/h, corresponding to the current driving patterns, sport, normal, and eco, set up by car manufacturers. A reduction of 10% in vehicle speed in urban and peripheral routes achieves a minimum energy rate, enhancing battery management. Current vehicle speed shows a deviation from optimum management of 18% while applying vehicle speed reduction limits the deviation to 0.2%. Experimental results show a good agreement with simulation data, with 94% accuracy. We tested the protocol for urban and peripheral routes with maximum vehicle speed limits of 60 and 90 km/h.

Keywords: hybrid electric vehicle; battery management; performance enhancement; energy consumption rate; vehicle speed



Citation: Armenta-Déu, C. Battery Management for Improved Performance in Hybrid Electric Vehicles. *Vehicles* **2024**, *6*, 949–966. <https://doi.org/10.3390/vehicles6020045>

Academic Editor: Yiqun Liu

Received: 9 April 2024

Revised: 22 May 2024

Accepted: 28 May 2024

Published: 31 May 2024



Copyright: © 2024 by the author. Licensee MDPI, Basel, Switzerland. This article is an open access article distributed under the terms and conditions of the Creative Commons Attribution (CC BY) license (<https://creativecommons.org/licenses/by/4.0/>).

1. Introduction

The replacement of internal combustion engine (ICE) cars with electric vehicles has occurred more slowly than expected for several reasons: higher cost, shorter driving range, and lack of a charging station network, especially in some countries [1]. Electric vehicles (EVs) can be categorized depending on the power source configuration into hybrid electric vehicles (HEVs), plug-in hybrid electric vehicles (PHEVs), battery electric vehicles (BEVs), and fuel cell electric vehicles (FCEVs) [2]. The disruption caused by a sudden unexpected vehicle stop because of a lack of available charging stations reduces people's motivation to buy a fully electric vehicle, even more so if the user must drive for long distances [3].

An alternative to the fully electric vehicle, BEV or FCEV, is the hybrid configuration, either PHEV or HEV. A new configuration derived from the HEV, the mild hybrid electric vehicle (MHEV), integrates the electric vehicle fleet offering. Hybrid electric vehicles have the advantage of low or no dependence on electric charging stations, especially the MHEV or HEV configuration, since they can run on fuel for an entire trip.

HEVs and MHEVs suffer from higher weights than ICE cars due to the battery, tending to reduce vehicle performance and shorten the driving range [4]. Indeed, increasing the vehicle mass produces a higher energy consumption rate, thus lowering the traveling distance for the same available energy. The higher performance of the electric motor, which has lower energy transmission losses, compensates for this drawback, resulting in a driving range extension compared to ICE cars [5].

The longer driving distance, however, depends on the driving pattern, the driver's attitude, and driving conditions. Considering equal driving conditions, the style of driving critically influences the energy consumption rate and the vehicle's driving range [6]. Previous studies demonstrate that high average speed and acceleration provoke a drastic increase in energy consumption [7] and therefore a significant reduction in vehicle autonomy [8,9].

Electric vehicle manufacturers offer a selection of driving modes to adapt the vehicle performance to the driver's attitude and expected style of driving for the different power source configurations. The selection currently includes sport, normal, and eco mode, corresponding to aggressive, conventional, and moderate styles of driving, respectively [10]. Unfortunately, drivers often do not use the appropriate driving mode, increasing the energy consumption rate [11].

Currently, the driver selects a driving mode, maintaining this driving mode forever or for long driving periods, days, or even weeks, independent of the traffic and route conditions. This is due to the driver's desire to have a specific response from the vehicle or because the driver does not pay much attention to traffic and route conditions, forgetting to change to a more efficient driving mode [12].

On the other hand, it has been found that drivers do not know much about the performance of an electric vehicle, whether it is a hybrid or not, and they doubt the convenience of changing from one driving mode to another to reduce the energy consumption rate, extending the driving range [13]. Due to this situation, drivers run electric vehicles in non-optimal conditions, wasting energy and lowering vehicle efficiency [14], which is especially significant in hybrid electric vehicles due to the safeguarding of the internal combustion engine that guarantees the continuous operation of the car and ensures the completion of the planned route.

The best solution to optimize the energy use in a battery electric vehicle is to disconnect the vehicle power source from the driver operation, thus avoiding interaction between the driver and the power management. The automatic control of driving operations enhances the vehicle performance, reduces the energy consumption rate, extends the driving range, and reduces greenhouse gas (GHG) emissions to the environment. Of course, manual operation selection is mandatory since the drivers must have vehicle control for security reasons like emergencies or unexpected traffic conditions.

Much effort and work has been devoted to enhancing energy management in electric vehicles, whether full-electric or hybrid, but most of these have set up a defined protocol without considering specific circumstances or driving history. Among these studies are those focused on developing algorithms to evaluate the battery performance [15]; optimizing the battery management system (BMS) to ensure an appropriate and secure battery operation [16]; dealing with power management to improve battery performance [17]; analyzing the battery parameters like the state of charge, temperature, equalization, etc., to make the battery operate in optimum conditions [18]; and evaluating the influence of battery management to achieve sustainable developments [19].

Another strategy is dealing with the energy management system (EMS) to evaluate the battery response to power demand from electric engines or ancillary equipment [20] and analyze the electric vehicle power sources [21]. Among the studies that use the EMS strategy, it is worth highlighting those that focus on consumption management, seeking to minimize energy use; our current study falls within this category.

In this study, we proposed a new method to improve battery management; the new method develops a protocol based on energy consumption rate optimization for every driving condition. The protocol considers the energy consumption rate as the parameter for automatically changing the driving mode. To this end, the protocol uses dynamic motion parameters like vehicle speed and acceleration and road characteristics such as pavement type and road slope. The protocol evaluates the energy consumption continuously and compares the result with the estimated value for optimum driving conditions according to

traffic characteristics and road restrictions, changing the driving mode or not depending on the comparison result.

2. Theoretical Foundations

In this section, we show the mathematical development to obtain the algorithm to control the battery management optimization. This mathematical development focuses on maximizing the extracted energy from the battery and, thus, the driving distance.

Energy consumption rate, ζ_r , is defined as the ratio of energy use, ζ , to traveled distance, d ; mathematically:

$$\zeta_r = \zeta / d \tag{1}$$

The energy use depends on the required power, P_t , and operating time, t_{op} , as in Equation (2).

$$\zeta = P_t t_{op} \tag{2}$$

Power requirements derive from applied force to propel the vehicle, F , and average speed, $\langle v \rangle$, according to:

$$P_t = F \langle v \rangle \tag{3}$$

Dynamic force includes inertial, drag, rolling, and weight force:

$$F = ma + \kappa v^2 + \mu mg + mg \sin \alpha \tag{4}$$

a and v are the acceleration and vehicle speed, m is the vehicle mass, κ and μ are the drag and rolling coefficient, and α is the road slope.

Combining the above Equations:

$$\zeta_r = \frac{(ma + \kappa v^2 + \mu mg + mg \sin \alpha) \langle v \rangle t_{op}}{d} \tag{5}$$

Because a route consists of segments with different dynamic and road conditions, Equation (5) should be transformed into:

$$\zeta_r = \sum_{i=1}^n \frac{\langle v_i \rangle t_{op,i}}{d_i} (ma_i + \kappa v_i^2 + \mu_i mg + mg \sin \alpha_i) \tag{6}$$

i accounts for the segment index.

Since the fraction in the summation is equal to 1:

$$\zeta_r = \sum_{i=1}^n (ma_i + \kappa v_i^2 + \mu_i mg + mg \sin \alpha_i) \tag{7}$$

The rolling and weight force in Equation (7) can be expressed in terms of equivalent acceleration; therefore, Equation (7) converts into:

$$\zeta_r = \sum_{i=1}^n (ma_{ef,i} + \kappa v_i^2) \tag{8}$$

where the equivalent acceleration is:

$$a_{ef,i} = a_i + \mu_i g + g \sin \alpha_i \tag{9}$$

To minimize the energy consumption rate, we should apply the first derivative. Nevertheless, since there are two variables, acceleration and speed, we must express the acceleration in terms of the vehicle speed; therefore:

$$a_{ef,i} = \frac{(v_{f,i})^2 - (v_{o,i})^2}{2d_i} \tag{10}$$

Sub-indexes *o* and *f* account for the initial and final vehicle speed in the segment, and *d_i* is the traveled distance for segment *i*.

On the other hand, we can express the vehicle speed in the drag term as:

$$v_i = \frac{v_{f,i} + v_{o,i}}{2} \tag{11}$$

Now, applying the first derivative, using the vehicle speed as the reference variable, developing the summations in Equation (7), considering that the initial speed of segment *i + 1* is the final speed of segment *i*, and grouping terms, we have:

$$v_o \left(2\kappa - \frac{m}{d_1} \right) + 4\kappa \sum_{i=1}^n \left[\frac{m}{4\kappa} v_{f,i} \left(1 + \frac{1}{d_i} - \frac{1}{d_{i+1}} \right) \right] + 2\mu g \sum_{i=1}^n d_i + 2g \sum_{i=1}^n d_i \sin \alpha_i = 0 \tag{12}$$

The last term in Equation (12) vanishes for flat terrain; thus:

$$v_o \left(2\kappa - \frac{m}{d_1} \right) + 4\kappa \sum_{i=1}^n \left[\frac{m}{4\kappa} v_{f,i} \left(1 + \frac{1}{d_i} - \frac{1}{d_{i+1}} \right) \right] + 2\mu g \sum_{i=1}^n d_i = 0 \tag{13}$$

d₁ corresponds to the first segment traveled distance, and *v_o* is the starting vehicle speed.

Rearranging Equation (12):

$$\frac{v_o}{4\kappa} \left(2\kappa - \frac{m}{d_1} \right) + \sum_{i=1}^n \left[\frac{m}{4\kappa} v_{f,i} \left(1 + \frac{1}{d_i} - \frac{1}{d_{i+1}} \right) \right] + \frac{\mu g}{2\kappa} \sum_{i=1}^n d_i + \frac{g}{2\kappa} \sum_{i=1}^n d_i \sin \alpha_i = 0 \tag{14}$$

We calculate the distance for every segment from the route pattern obtained from a navigation map (Google Maps [22], Geo Tracker [23], Petal Maps [24], Sygic [25], Waze [26], or any other); therefore, the only remaining variable is the vehicle speed.

Provided the starting vehicle speed is known, we determine the first term in Equations (12) and (13) from the vehicle characteristics; therefore:

$$\sum_{i=1}^n \left[\frac{m}{4\kappa} v_{f,i} \left(1 + \frac{1}{d_i} - \frac{1}{d_{i+1}} \right) \right] + \frac{\mu g}{2\kappa} \sum_{i=1}^n d_i + \frac{g}{2\kappa} \sum_{i=1}^n d_i \sin \alpha_i = C_o \tag{15}$$

where coefficient *C_o* is:

$$C_o = v_o \left(\frac{m}{4\kappa d_1} - \frac{1}{2} \right) \tag{16}$$

Equation (15) defines the control algorithm for optimizing the battery management.

For the simulation process, we compare the calculated value from the left and the right side of Equation (15).

3. Energy Management

Energy consumption in a hybrid electric vehicle derives from the fuel and battery supply; the battery represents the traction system (series hybrid) or supplies power in combination with the ICE (parallel hybrid), depending on the vehicle configuration [27]. In the first mode, the battery receives energy from the electric generator powered by the ICE. In the second mode, the internal combustion engine and the electric motor, powered by the battery, are mechanically connected to the transmission and can directly power the vehicle. The vehicle can operate on either the internal combustion engine, the electric motor, or by combining both power sources.

Electric vehicles (EVs) and hybrid electric vehicles (HEVs) depend heavily on battery management systems (BMS). Essentially the brains and heart of these cars, the BMS keeps an

eye on the battery pack and regulates it while guaranteeing longevity, safety, dependability, and peak performance.

Three types of battery management systems operate in hybrid electric vehicles: centralized, distributed, and modular [28]. Figure 1 shows the schematic representation of every system.

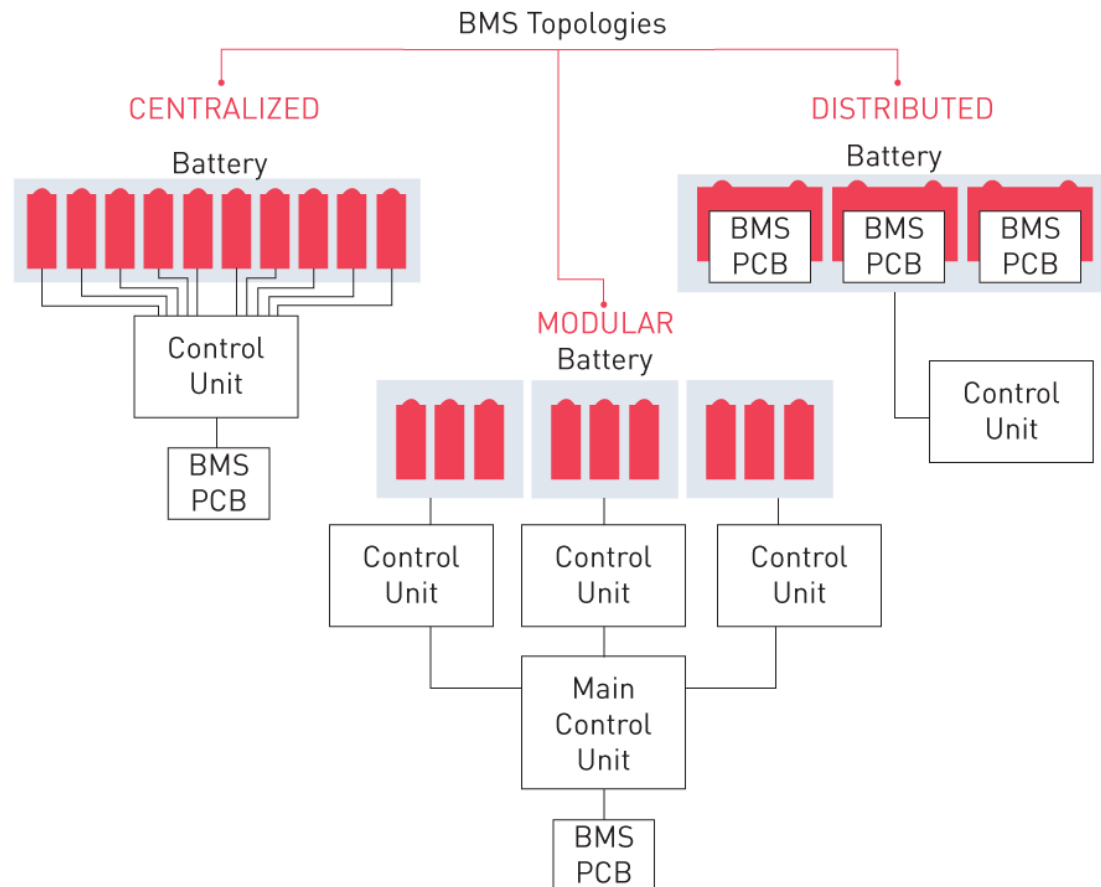


Figure 1. Schematic representation of BMS for HEVs.

The strategy of the battery management system depends on the EV manufacturer. Toyota applies the following protocol: in slow-moving traffic, the generator can cut out the petrol engine and let the electric motor take over for zero-emissions traveling [29]. To charge the battery, the BMS continuously monitors the voltage; below a threshold, the electric generator, powered by the ICE, charges the battery. Additionally, the regenerative braking system charges the battery when braking or decelerating. Hyundai hybrid electric vehicles similarly use the BMS, although some differences arise [30]; depending on the driving situation, BMS switches seamlessly between its petrol engine and electric motor. The regenerative braking system charges the battery using the electric motor to slow the car. The energy stored in the battery then powers the electric motor to help in acceleration, uphill driving, and low-speed driving. Renault BMS operates differently [31]; hybrid cars start with 100% electric power, which continues during the first few miles to offer a more lively pick-up. Under the combined electric and combustion engine types, hybrids can drive in electric mode most of the time. Nevertheless, E-Tech technology captures more energy than most hybrids; therefore, the user can drive in electric mode for as long as possible. When the battery lacks enough power, the combustion engine comes to the rescue and offers full hybrid traction, with the two power sources running simultaneously.

Other electric vehicle manufacturers similarly operate the BMS to the above methodologies. BMS maintains the battery state of charge (SOC) between limits, currently 20% to 80% [32].

Since the battery management system is responsible for preserving a safe and operational state of charge, and because of the close relation between the battery and internal combustion engine operability, any operation form reflects on the energy consumption rate. Indeed, if we apply Equation (2), the required energy to traction the hybrid electric vehicle comes from the ICE or the battery; however, the mechanical transmission from engine to wheel is different depending on the power source, ICE, or battery.

Considering the necessary energy for vehicle traction, we have:

$$\xi_{pw} = \xi_{wh} / \eta_t \tag{17}$$

Sub-indexes *pw* and *wh* account for the power source and wheel. η_t is the transmission efficiency.

Considering a hybrid electric vehicle operates partially in the electric mode, the required energy from the power source is:

$$\xi_{comb} = F_{ICE} \frac{\xi_{ICE}}{\eta_{mech}} + F_{bat} \frac{\xi_{bat}}{\eta_{el}} \tag{18}$$

F_{bat} and F_{ICE} are the fractions of demanded energy supplied by the battery and internal combustion engine, and η_{mech} and η_{el} are the mechanical and electric transmission efficiency.

Since the battery charges from the ICE through an electric generator, the energy injected into the battery depends on the generator’s efficiency; therefore:

$${}^{in}\xi_{bat} = {}^{bat}\xi_{ICE}\eta_{gen} \tag{19}$$

${}^{bat}\xi_{ICE}$ and ${}^{in}\xi_{bat}$ represent the output energy from the ICE and input energy into the battery, and η_{gen} is the generator efficiency.

On the other hand, the power extraction from the battery suffers from energy losses; therefore:

$$\xi_{bat} = {}^{out}\xi_{bat} = {}^{in}\xi_{bat}\eta_{bat} \tag{20}$$

Combining Equations (18) and (19) and replacing in Equation (17):

$$\xi_{comb} = \xi_{ICE} \left[F_{bat} \left(\frac{\eta_{el} - \eta_{mech}\eta_{gen}\eta_{bat}}{\eta_{el}\eta_{mech}} \right) + \frac{\eta_{gen}\eta_{bat}}{\eta_{el}} \right]^{-1} \tag{21}$$

Retrieving data from the literature, we obtain electric, mechanic and generator efficiency [33], and battery performance [34]. From these values, we can determine the combined energy consumption as a function of the operational electric mode fraction.

If we divide by time, Equation (21) converts into:

$$\left. \frac{\xi_{comb}}{\xi_{ICE}} \right|_r = \left[F_{bat} \left(\frac{\eta_{el} - \eta_{mech}\eta_{gen}\eta_{bat}}{\eta_{el}\eta_{mech}} \right) + \frac{\eta_{gen}\eta_{bat}}{\eta_{el}} \right]^{-1} \tag{22}$$

Equation (22) expresses the energy consumption ratio when using a combined battery and ICE power source related to an internal combustion engine.

Energy Consumption Simulation

Provided the efficiencies in Equation (21) are known, we can determine the energy consumption as a function of the power fraction supplied by the battery. Using the literature database, we have (Table 1):

Table 1. Efficiencies in a hybrid electric vehicle.

η_{el}	η_{mech}	η_{gen}	η_{bat}
0.855	0.65	0.9	0.95

Figure 2 shows the evolution of the ζ_{comb}/ζ_{ICE} ratio as a function of the battery use fraction.

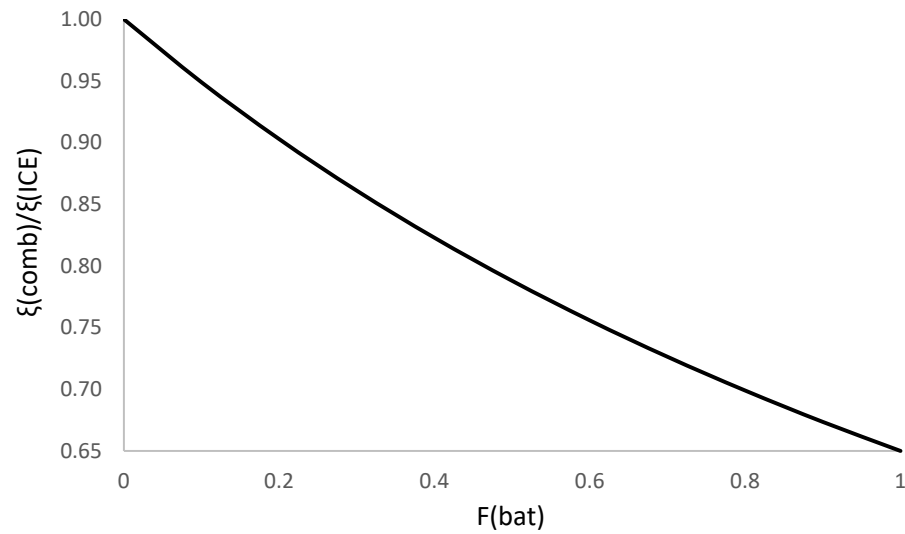


Figure 2. Evolution of the ζ_{comb}/ζ_{ICE} ratio as a function of the battery use fraction.

We observe how increasing the battery use as a source reduces the energy consumption rate, which may reach up to 35% for full-use battery use.

4. Simulation

To analyze the protocol, we run a simulation based on the algorithm of Equation (21). We use a light-duty vehicle as a reference. Table 2 lists the main characteristics of the vehicle.

Table 2. Vehicle characteristics.

Mass (kg)	1326
Aerodynamic coefficient: C_x	0.29
Front area: A_f (m ²)	2.52

We calculate the drag coefficient from the aerodynamic coefficient, C_x , using the following Equation:

$$\kappa = \frac{1}{2} \rho_{air} A_f C_x = \frac{1}{2} (1.225) (2.52) (0.29) = 0.45 \tag{23}$$

For the simulation, we have considered a variable starting vehicle speed and segment distance, up to 50 km/h (31.25 mph) and 1 km (0.625 miles), in steps of 10 km/h (6.25 mph) and 100 m (0.0625 miles). We establish the upper and lower limit of the starting vehicle speed according to current practice driving conditions. The initial segment distance extends to 1 km (0.625 miles) to cover a wide range.

To run the simulation, we propose a standard urban route composed of horizontal, uphill, and downhill segments, with variable speeds for everyone. Figure 3 shows the graphic representation of the simulated route.

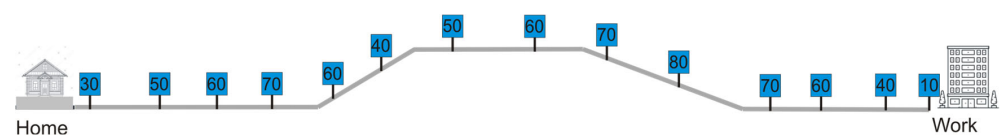


Figure 3. Schematic representation of the simulated urban route.

Labels in Figure 3 indicate the vehicle speed at the end of the segment for standard road traffic in a daily urban route. These values correspond to the recommended speed limitation according to traffic rules dictated by local authorities. The vehicle identifies the speed limitation using a camera that points to the speed traffic limit signal next to the road. We use these values as a reference for the simulation. The group of measures extends for 213 days for the same urban route and similar traffic conditions [35]. In the simulation, we use values from daily driving conditions to reproduce a current situation, representing a faithful panorama.

According to local regulations in many cities, the traffic speed limit is 50–70 km/h in urban routes, including peripheral zones [36]. Since the traffic regulations change depending on the country, we averaged values for two zones, within towns (50 km/h) and interurban roads (90) km/h. The peripheral route represents an intermediate road between urban and interurban; therefore, we estimate the speed limit as 70 km/h, taken as the reference value. The 80 km/h value corresponds to a temporary vehicle speed due to the inertial effects in the route downhill section. We assume that this speed limit overpassing is compatible with traffic rules due to the low-speed excess and the short time it lasts.

We divide the urban route into 14 segments for a total distance of 17.1 km (10.7 miles). The total distance corresponds to the worldwide average daily driving distance considering a one-way trip [37].

Table 3 shows the distance distribution for the one-way route. We obtain the values averaging data from a statistical analysis of daily trips run by drivers in urban zones [37].

Table 3. Daily route distance distribution by segment (first round).

Segment	1	2	3	4	5	6	7
Distance (m)	350	1550	950	850	1750	1250	1950
Distance (miles)	0.219	0.969	0.594	0.531	1.094	0.781	1.219
Segment	8	9	10	11	12	13	14
Distance (m)	1350	1450	1150	2250	750	950	550
Distance (miles)	0.844	0.906	0.719	1.406	0.469	0.594	0.344

The average value of this test for the whole route is 40.8 km/h (25.5 mph).

Figure 4 shows the evolution of the coefficient C_0 as a function of the initial segment distance and starting vehicle speed.

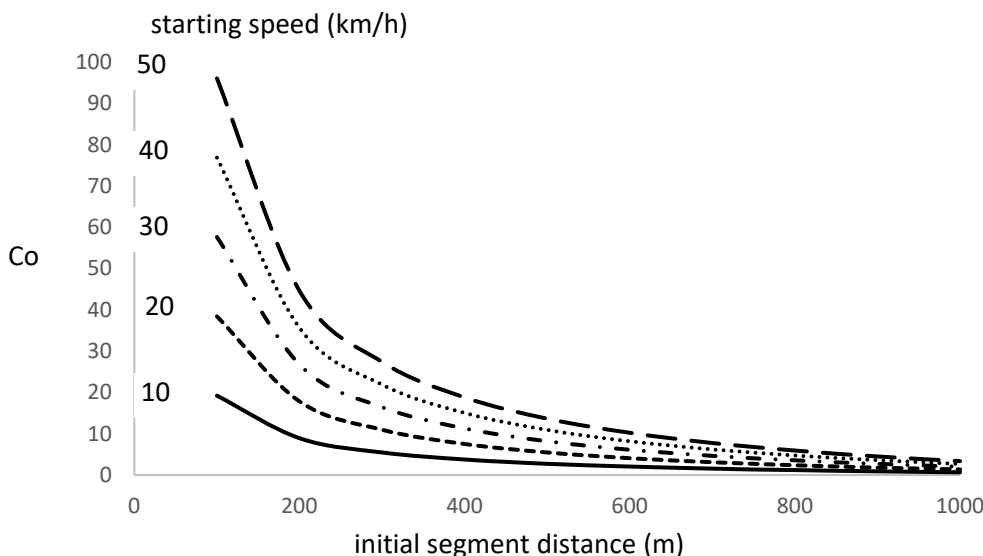


Figure 4. Evolution of coefficient C_0 as a function of starting vehicle speed and initial segment distance.

We notice that the coefficient C_0 rapidly raises for low initial segment distance, below 200 m, and merges to a unique value as the initial segment distance increases. The increase in the C_0 coefficient for short initial segment distance is faster as the starting vehicle speed increases. We deduce that the minimum energy consumption rate condition, imposed by Equation (21), is more sensitive to short initial segment distance and high starting vehicle speed.

Applying values from Tables 2 and 3 to Equation (21) for every segment, we obtain the following results (Figure 5):

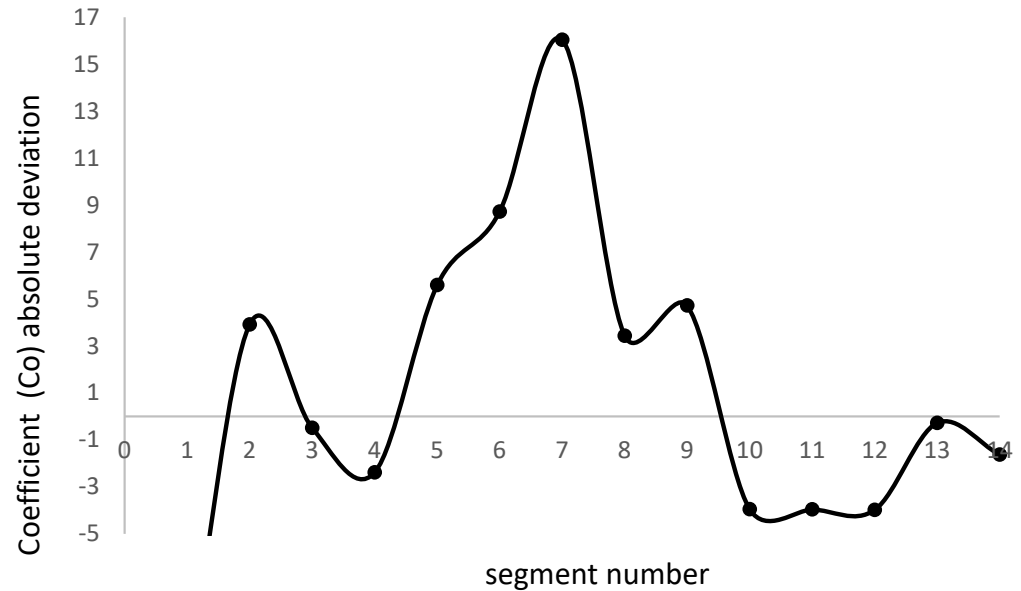


Figure 5. Absolute deviation of coefficient C_0 .

From C_0 deviation values, we can determine the excess energy consumption rate related to the optimum value. To do so, we calculate the relative quadratic error for every segment, obtaining (Figure 6):

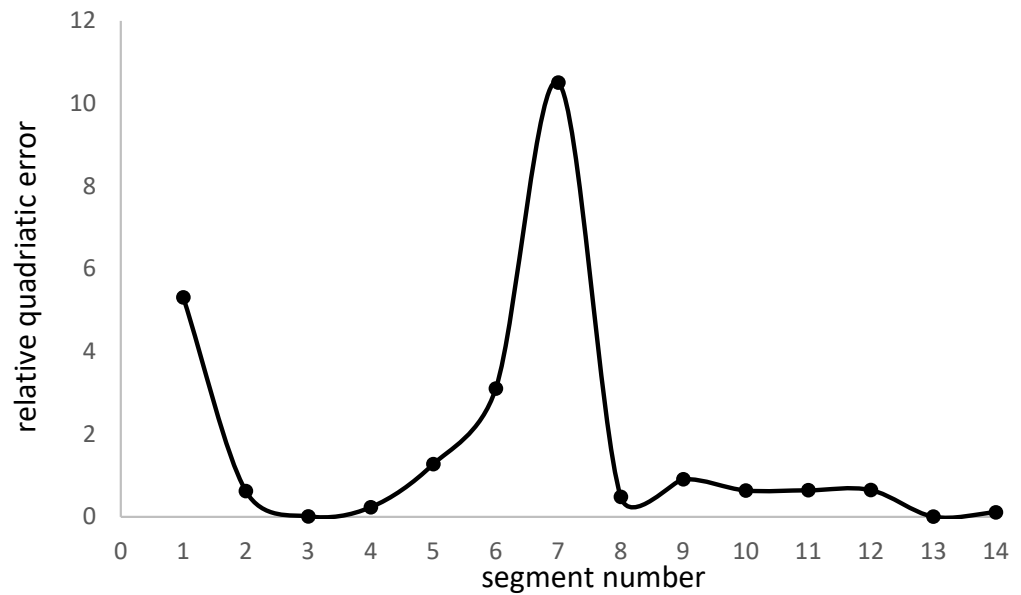


Figure 6. Relative quadratic error for the coefficient C_0 .

The graph displays the coefficient C_o 's solid line, which determines the accuracy of achieving the minimum energy consumption rate, ζ_r . It is evident from the black dots representing segment values that there is a deviation, indicating the suboptimal performance of the hybrid electric vehicle's driving mode. The deviation value quantifies how far the driving mode falls from the optimal mode, with higher deviation values indicating lower efficiency of the HEV.

We realize that the highest quadratic error values correspond to segments 1, 6, and 7. Segment 1 accounts for the vehicle starting with a high acceleration process, and segments 6 and 7 correspond to the uphill section. We, therefore, conclude that acceleration and maintaining vehicle speed in the uphill section represent the most penalizing processes for the energy consumption rate.

The analysis of results from Figure 5 shows that the maximum deviation accounts for segments 5 to 7, corresponding to the uphill route section where power requirements increase. Therefore, we conclude that the energy consumption rate diverges from the optimum value with power demand.

We realize that, for many segments, the relative quadratic error is near zero, which indicates that the driving conditions are close to the optimum performance. Segment 3 matches the condition of null error, meaning the vehicle operates at optimum performance for this segment's driving conditions. For segments 8 to 14, the energy consumption rate is higher than optimum, thus generating fuel overconsumption and operating the battery at poorer management.

At the beginning of the route and uphill segments, the relative error is high, which indicates that the energy consumption rate is much higher than expected and not at its optimum value. One reason for this could be the acceleration rate at the start of the journey, which needs to be lowered. Also, maintaining the vehicle speed on uphill roads can cause fuel overconsumption, negatively impacting energy consumption and battery energy management.

Since the energy consumption rate directly relates to power management efficiency, the lower the ζ_r value, the higher the efficiency. On the other hand, because the energy consumption rate includes battery energy management, a high value of the ζ_r parameter means poor battery management and vice versa. Therefore, to achieve an optimum battery energy management process, the deviation of the C_o coefficient should be null for every route segment.

The correction of the deviation of the C_o coefficient implies modifying the vehicle speed at every segment to match a null deviation.

We achieve this goal by correcting the vehicle speed until the deviation becomes null. The correction factor is 0.9 for the simulated case, but it changes when modifying driving conditions like the route profile, segment distribution, and vehicle speed at every segment. This coefficient applies to urban and peripheral routes with a speed limitation of 50 km/h and 70 km/h.

If the vehicle exceeds the speed limit indicated above, the correction coefficient must be modified by an additional 0.1 for each additional 10 km/h in which the established speed limit exceeds; therefore, for a speed of 80 km/h, the coefficient should be 0.2, for 90 km/h, 0.3, and so on.

Figure 7 shows the relative quadratic error after applying the correction factor to the vehicle speed.

We notice the relative error is low, 0.16 on average, and below 0.4 for all segments except number 7, corresponding to the maximum vehicle speed during the uphill road section. The low error warrants the improvement of battery management since the energy consumption rate lowers. The correction algorithm may modify the vehicle speed until reaching the expected relative error to reduce the deviation in segment 7 to match the average value; nevertheless, if the resulting vehicle speed is too low for warranting secure driving conditions, the program maintains the correction factor even that the vehicle speed penalizes the global energy consumption and the battery power management.

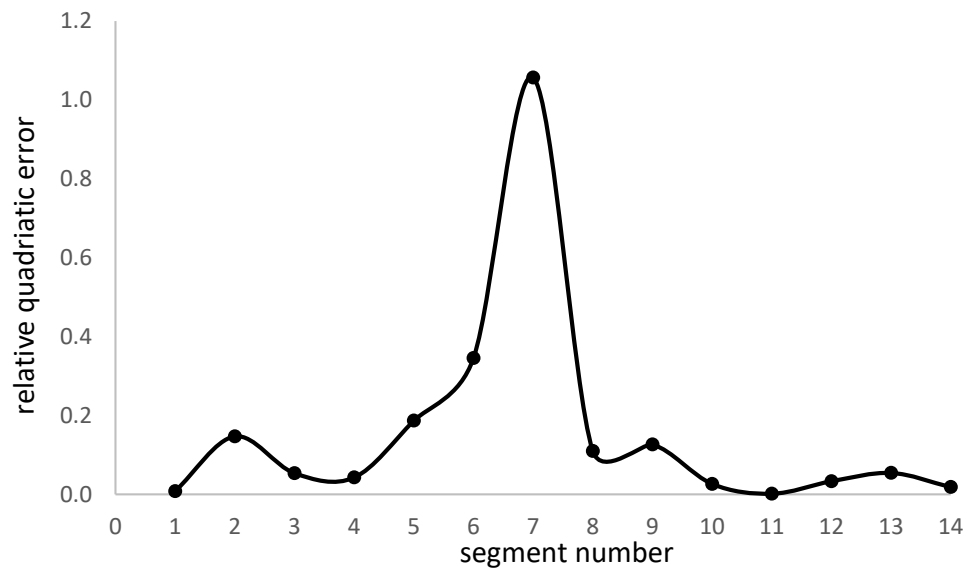


Figure 7. Corrected absolute deviation of coefficient C_0 .

Now, comparing the relative quadratic error for corrected and non-corrected vehicle speed, we have (Figure 8):

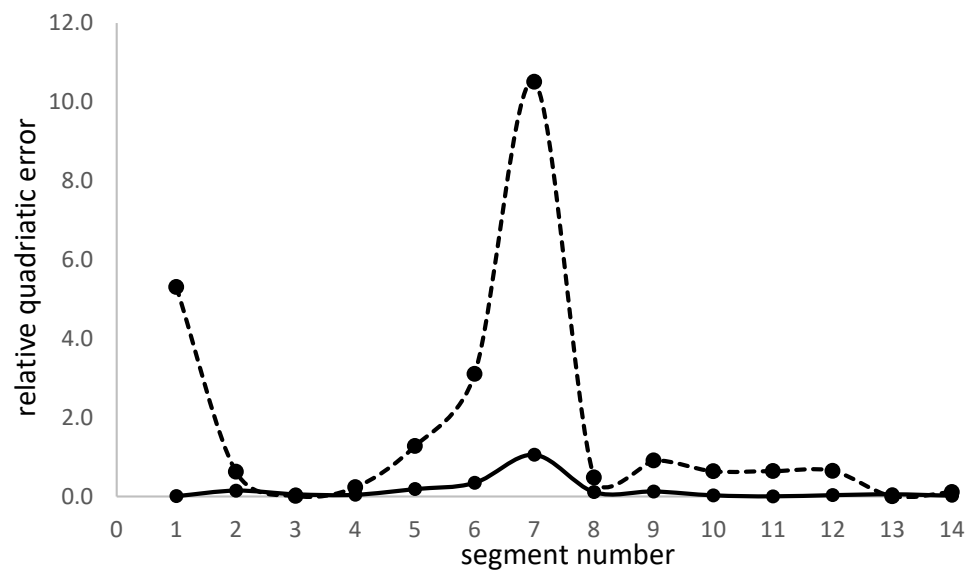


Figure 8. Corrected (solid line) and non-corrected (dashed line) relative quadratic error of coefficient C_0 .

We observe a noticeable reduction in the relative quadratic error when applying the vehicle speed lowering, a sign of the effectiveness of the proposed action on the energy consumption rate.

To reinforce the analysis developed for the previous urban route, we ran a second test in a flat-terrain urban route with different segment numbers and vehicle speeds. Figure 9 shows the driving profile of the urban route for the second test.

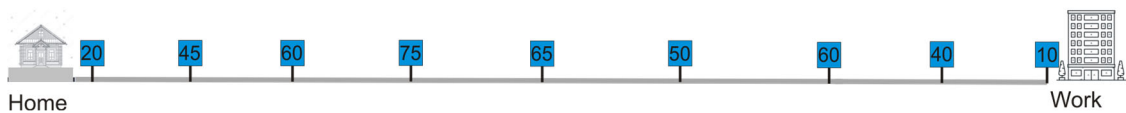


Figure 9. Schematic representation of the simulated flat terrain urban route.

As in the case of Figure 3, labels in Figure 9 indicate the vehicle speed at the end of the segment for standard road traffic in a daily urban route.

We divide this second urban route into nine segments for the same global distance of 17.1 km (10.7 miles). Table 4 shows the distance distribution for the one-way route. We obtain the values averaging data from a statistical analysis of daily trips run by drivers in urban zones [38].

Table 4. Daily route distance distribution by segment (second round).

Segment	1	2	3	4	5	6	7	8	9
Distance (m)	350	1550	1650	2250	2750	2300	2750	1750	1750
Distance (miles)	0.219	0.969	1.031	1.406	1.719	1.438	1.719	1.094	1.094

The average value of this second test for the whole route is 57.9 km/h (36.2 mph).

Figure 10 shows the evolution of the coefficient C_o as a function of the initial segment distance and starting vehicle speed.

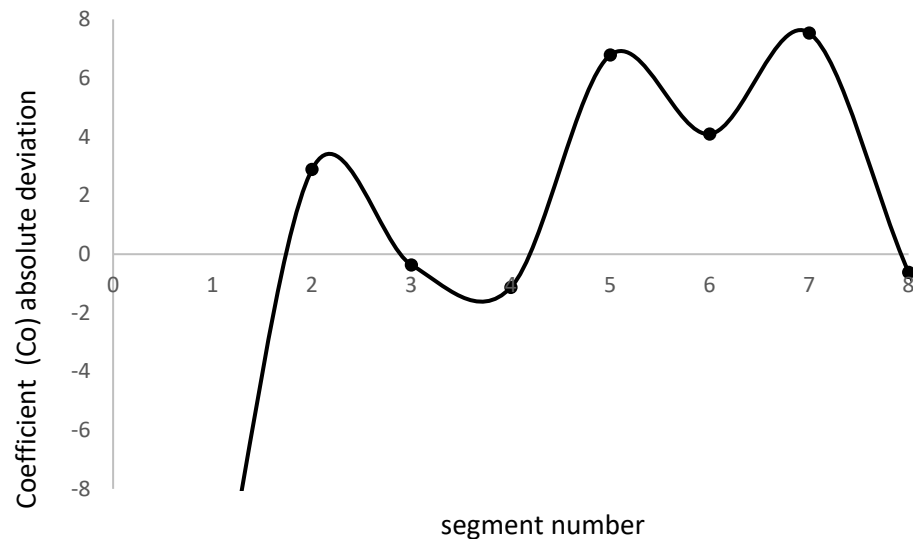


Figure 10. Absolute deviation of coefficient C_o (flat terrain).

Comparing with the first test, we obtain (Figure 11):

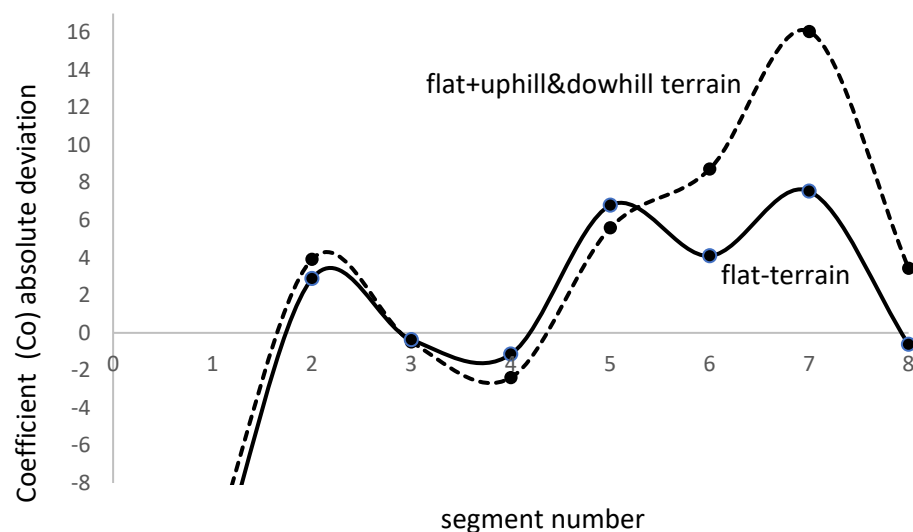


Figure 11. Comparison of absolute deviation of coefficient C_o .

We observe that the absolute deviation is very close while the terrain is flat, segments 1 to 5, but diverges as soon as the terrain changes to uphill orography. We reduce the comparison to the first 8 segments, which include a flat terrain and an uphill section.

Figure 12 shows the relative quadratic error associated with the second test.

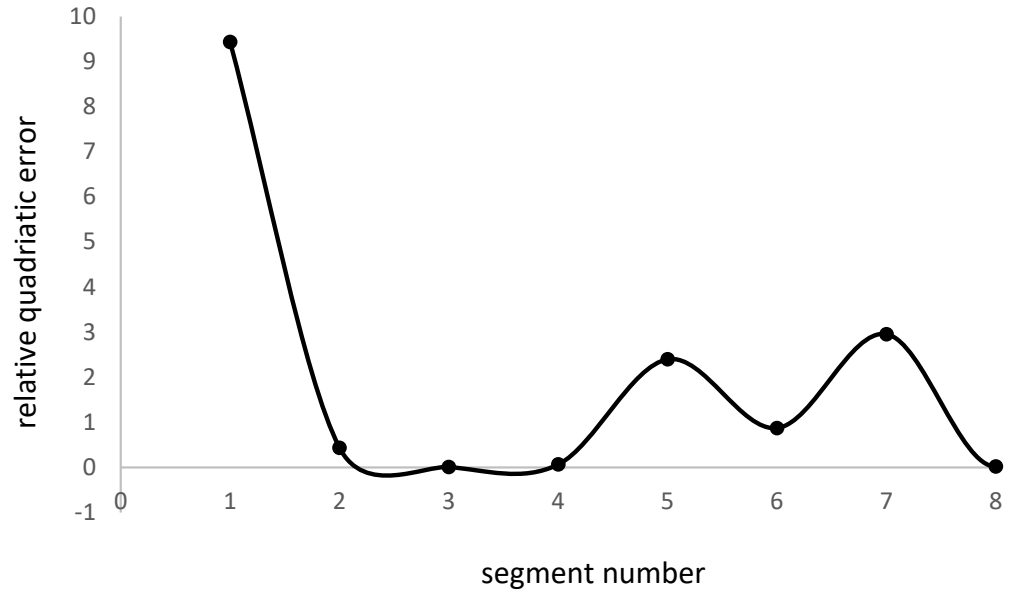


Figure 12. Relative quadratic error for the coefficient C₀ (flat terrain).

The apparent negative values between points 2 and 4 in Figure 12 are a drawing problem since they do not correspond to negative values; drawing between points 2 and 4 should be a horizontal line with values identically zero.

Repeating the comparative analysis for corrected and non-corrected vehicle speed, we obtain (Figure 13):

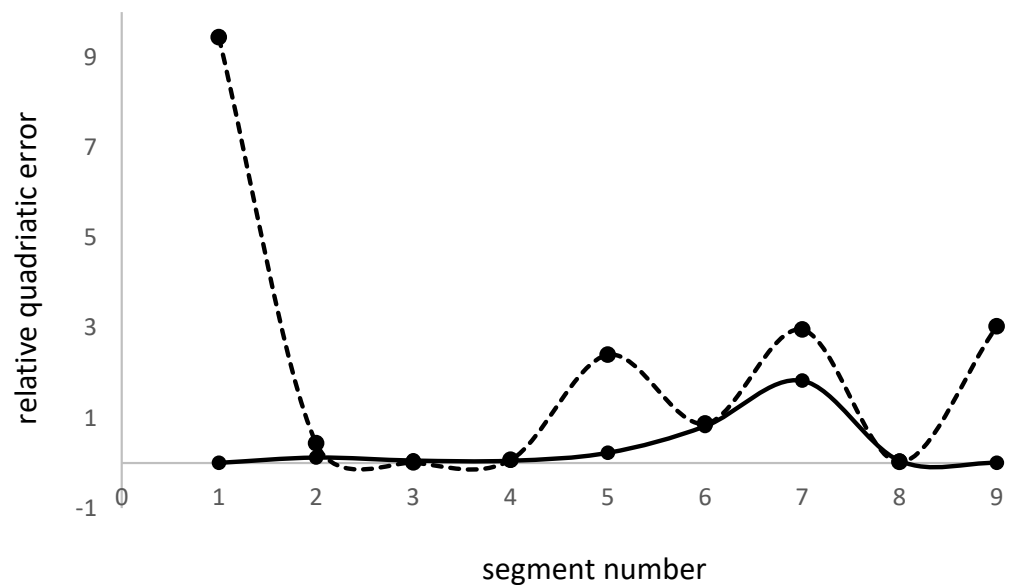


Figure 13. Corrected (solid line) and non-corrected (dashed line) relative quadratic error of coefficient C₀ (flat terrain).

As for Figure 13, the apparent negative values between points 2 and 4 are a drawing problem since they do not correspond to negative values; drawing between points 2 and 4 should be a horizontal line with values identically zero.

As in the first case, the vehicle speed reduction application reduces the relative quadratic error. This reduction means that the vehicle performance and battery management are enhanced.

5. Experimental Tests

We run experimental tests in a light-duty vehicle of identical characteristics, as mentioned in the simulation process, to verify the validity of the proposed methodology. The first group of tests aims to determine the evolution of the ζ_{comb}/ζ_{ICE} ratio as a function of the battery use fraction, as reflected in Figure 2.

Since driving conditions may vary during the route, we have determined the battery fraction used as the ratio between the time the vehicle operates in electric mode and the global time. The method is applied for 213 days, driving the same route at the same hours to maintain regular driving conditions for the entire group of tests. Table 5 shows the traveled distance for every battery fraction used.

Table 5. Test characteristics.

F_{bat}	0	0.1	0.2	0.3	0.4	0.5
Distance (km)	99.8	98.0	101.5	92.8	94.5	109.4
Distance (miles)	62.3	61.3	63.4	58.0	59.1	68.4
F_{bat}	0.6	0.7	0.8	0.9	1	
Distance (km)	91.9	100.6	96.3	87.5	105.0	
Distance (miles)	57.4	62.9	60.2	54.7	65.6	

Electric vehicle software (RT-01v24) provides the battery fraction use value and the traveled distance at the end of every route. The process collects data by adding the values for the selected battery fraction to obtain the traveled distance.

Equation (1) allows for determining the energy consumption rate in experimental tests; the electric vehicle computer provides the fuel consumption and the traveled distance. Figure 14 shows the comparative analysis between simulated data and experimental results for the energy consumption rate:

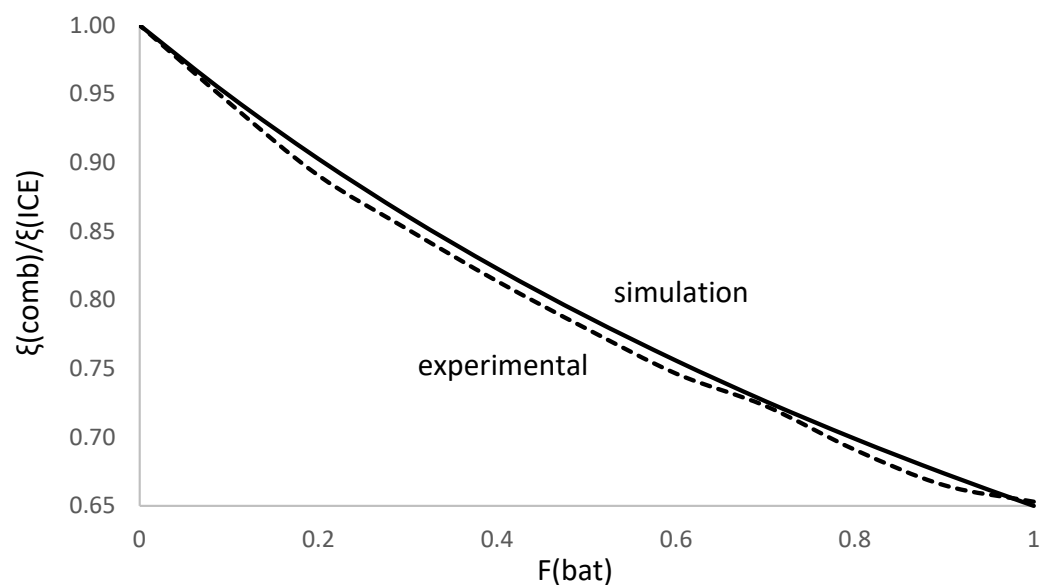


Figure 14. Correlation between simulation data and experimental results of energy consumption rate for a variable fraction of battery use as a power source.

The comparative analysis in Figure 14 shows a good agreement between experimental results and simulated data for the calculation method provided in Equation (21).

The accuracy of predicting energy consumption rate is 99.1%, proving the validity of the proposed algorithm.

Applying the driving conditions established in Figure 3, we run experimental tests to evaluate the coefficient C_o in current driving conditions. The cruise control sets up the experimental vehicle speed, and the vehicle computer regulates the distance. A slight delay occurs when changing from one speed to another since the change is manual; however, the traveled distance during the transient time is low compared to the segment distance, below 4% in all cases. Table 6 shows the transient distance for every vehicle speed change in route type I (flat plus uphill and downhill terrain).

Table 6. Absolute and relative transient distance in vehicle speed change (urban route type I).

Segment	1	2	3	4	5	6	7
Absolute distance (km)	13.3	23.6	30.0	31.1	26.7	27.8	20.8
Relative distance (%)	3.8	1.5	3.2	3.7	1.5	2.2	1.1
Segment	8	9	10	11	12	13	14
Absolute distance (km)	31.7	29.2	33.3	48.6	25.0	24.4	6.1
Relative distance (%)	2.3	2.0	2.9	2.2	3.3	2.6	1.1

The results of experimental tests for the coefficient C_o evolution with starting vehicle speed are shown in Figure 15.

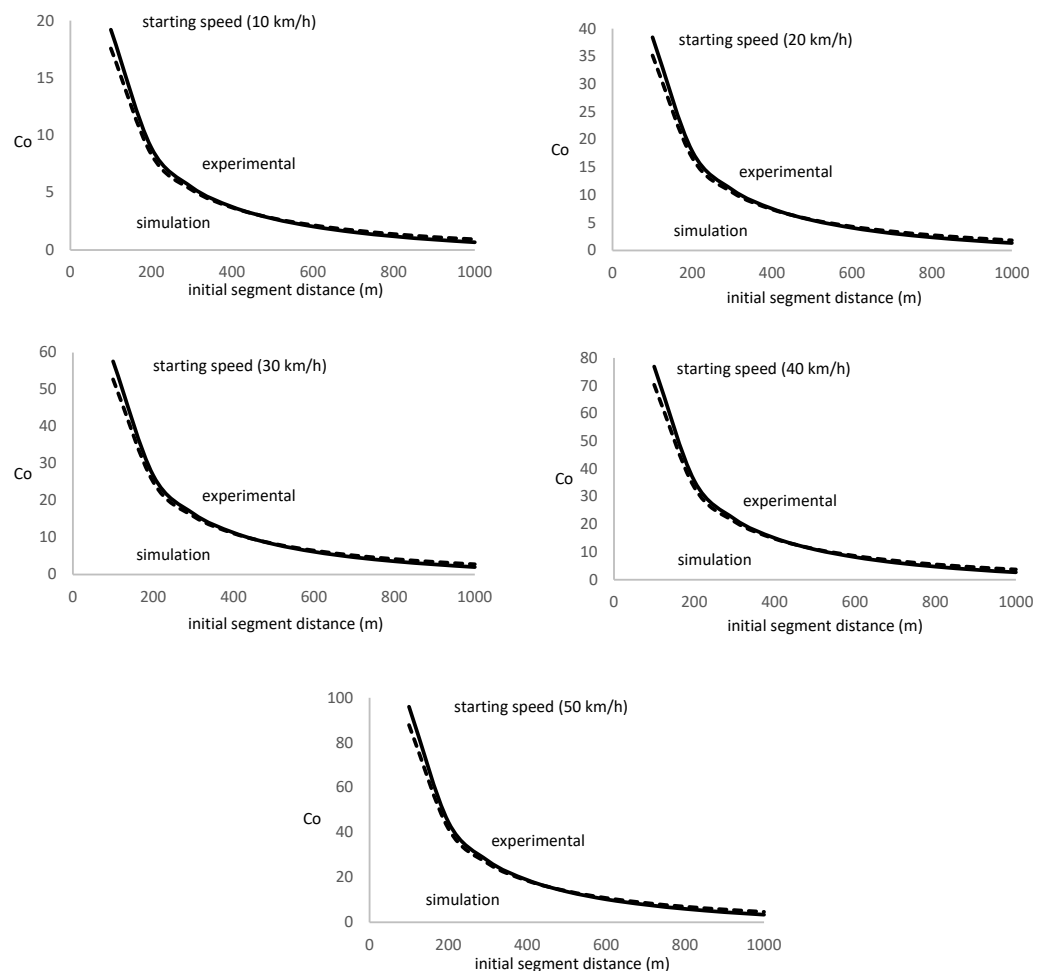


Figure 15. Comparison between experimental results and simulation data of the coefficient C_o for the urban route type I (flat, uphill and downhill terrain).

Experimental results show a good agreement with simulation prediction, with 94% accuracy. The comparative analysis shows a slight overestimation for low distance values at the initial traveling segment and a slight underestimation for the high one.

6. Conclusions

We present a protocol based on proposed algorithms focused on battery management performance enhancement. The protocol looks to minimize the energy consumption rate in hybrid electric vehicles, reducing the fuel consumption. Battery management is associated with fuel consumption and energy use, so the lower the energy use, the better the battery management.

The protocol based on the developed algorithms uses vehicle speed as the reference parameter to minimize energy use and optimize battery management. It also computes traveling distance for route segments using data from a navigation application for the specific route.

The study concludes that reducing vehicle speed by 10% in urban routes optimizes the energy consumption rate. If the vehicle overpasses the recommended traffic speed, we must increase the reduction by 10% for every 10 km/h overpassing.

Energy use and battery management deviation is only 0.2% from the optimum value when applying the speed reduction, while in current conditions, the deviation rises to 18%.

The protocol applies to urban and peripheral routes for daily trips. Although developed for moderate one-way traveling distances, the protocol applies to any distance, even back-and-forth daily trips.

The algorithm that rules the protocol for battery management optimization uses the vehicle mass and aerodynamic and rolling coefficient as variables to determine the minimum energy use and optimum battery management for specific driving conditions; therefore, it applies to any hybrid electric vehicle type and route characteristics.

The analysis applies to flat, uphill, and downhill terrain with maximum vehicle speed up to 90 km/h, a current value for peripheral routes in modern cities. In the present study, we limited the vehicle speed in downtown urban routes to 60 km/h.

The developed protocol has been tested for starting vehicle speed from 10 to 50 km/h, considering the three typical driving patterns, aggressive, moderate, and conservative, corresponding to sport, normal, and eco driving modes set up by car manufacturers.

Funding: This research received no external funding.

Data Availability Statement: Data are available from the author on request.

Conflicts of Interest: The authors declare no conflicts of interest.

References

1. Boulanger, A.G.; Chu, A.C.; Maxx, S.; Waltz, D.L. Vehicle electrification: Status and issues. *Proc. IEEE* **2011**, *99*, 1116–1138. [[CrossRef](#)]
2. National Research Council, Transportation Research Board, Division on Engineering, Physical Sciences, Board on Energy, Environmental Systems, & Committee on Overcoming Barriers to Electric-Vehicle Deployment. *Overcoming Barriers to Deployment of Plug-in Electric Vehicles*; National Academies Press: Washington, DC, USA, 2015.
3. Coffman, M.; Bernstein, P.; Wee, S. Electric vehicles revisited: A review of factors that affect adoption. *Transp. Rev.* **2017**, *37*, 79–93. [[CrossRef](#)]
4. Jung, H. Fuel economy of plug-in hybrid electric and hybrid electric vehicles: Effects of vehicle weight, hybridization ratio and ambient temperature. *World Electr. Veh. J.* **2020**, *11*, 31. [[CrossRef](#)]
5. Roshandel, E.; Mahmoudi, A.; Kahourzade, S.; Yazdani, A.; Shafiullah, G.M. Losses in efficiency maps of electric vehicles: An overview. *Energies* **2021**, *14*, 7805. [[CrossRef](#)]
6. Badin, F.; Le Berr, F.; Briki, H.; Dabadie, J.C.; Petit, M.; Magand, S.; Condemine, E. Evaluation of EVs energy consumption influencing factors, driving conditions, auxiliaries use, driver's aggressiveness. *World Electr. Veh. J.* **2013**, *6*, 112–123. [[CrossRef](#)]
7. Galvin, R. Energy consumption effects of speed and acceleration in electric vehicles: Laboratory case studies and implications for drivers and policymakers. *Transp. Res. Part D Transp. Environ.* **2017**, *53*, 234–248. [[CrossRef](#)]
8. Graba, M.; Mamala, J.; Bieniek, A.; Sroka, Z. Impact of the acceleration intensity of a passenger car in a road test on energy consumption. *Energy* **2021**, *226*, 120429. [[CrossRef](#)]

9. Ahn, K.; Rakha, H.; Trani, A.; Van Aerde, M. Estimating vehicle fuel consumption and emissions based on instantaneous speed and acceleration levels. *J. Transp. Eng.* **2002**, *128*, 182–190. [[CrossRef](#)]
10. Driving Modes Available in Electric Vehicles. Electric Vehicles. September 30, 2021 Driving Modes Available in Electric Vehicles. Available online: <https://iwheels.co> (accessed on 3 April 2024).
11. Karanam, V.; Davis, A.; Sugihara, C.; Sutton, K.; Tal, G. From shifting gears to changing modes: The impact of driver inputs on plug-in hybrid electric vehicle energy use & emissions. *Transp. Res. Interdiscip. Perspect.* **2022**, *14*, 100597. [[CrossRef](#)]
12. The Difference between Driving Modes Explained. The Difference between Driving Modes Explained | Motorama. Available online: <https://www.motorama.com.au/blog/motoring-tips/different-driving-modes> (accessed on 3 April 2024).
13. EV Explainer: Do Driving Modes Matter in Electric Vehicles? EV Explainer: Do Driving Modes Matter in Electric Vehicles? Available online: <https://thedriven.io> (accessed on 3 April 2024).
14. Sugihara, C.; Sutton, K.; Davis, A.; Karanam, V.; Tal, G. From sport to eco: A case study of driver inputs on electric vehicle efficiency. *Transp. Res. Part F Traffic Psychol. Behav.* **2021**, *82*, 412–428. [[CrossRef](#)]
15. Lipu, M.H.; Hannan, M.A.; Karim, T.F.; Hussain, A.; Saad MH, M.; Ayob, A.; Mahlia, T.I. Intelligent algorithms and control strategies for battery management system in electric vehicles: Progress, challenges and future outlook. *J. Clean. Prod.* **2021**, *292*, 126044. [[CrossRef](#)]
16. Mishra, S.; Swain, S.C.; Samantaray, R.K. A Review on Battery Management system and its Application in Electric vehicle. In Proceedings of the 2021 International Conference on Advances in Computing and Communications (ICACC), Kochi, India, 21–23 October 2021; IEEE: Piscataway, NJ, USA, 2021; pp. 1–6.
17. Sakhdari, B.; Azad, N.L. An optimal energy management system for battery electric vehicles. *IFAC-Pap.* **2015**, *48*, 86–92. [[CrossRef](#)]
18. Hannan, M.A.; Hoque, M.M.; Hussain, A.; Yusof, Y.; Ker, P.J. State-of-the-art and energy management system of lithium-ion batteries in electric vehicle applications: Issues and recommendations. *IEEE Access* **2018**, *6*, 19362–19378. [[CrossRef](#)]
19. Lipu, M.S.H.; Mamun, A.A.; Ansari, S.; Miah, M.S.; Hasan, K.; Meraj, S.T.; Abdolrasol, M.G.M.; Rahman, T.; Maruf, M.H.; Sarker, M.R.; et al. Battery management, key technologies, methods, issues, and future trends of electric vehicles: A pathway toward achieving sustainable development goals. *Batteries* **2022**, *8*, 119. [[CrossRef](#)]
20. Rimpas, D.; Kaminaris, S.D.; Aldarraji, I.; Piromalis, D.; Vokas, G.; Papageorgas, P.G.; Tsaramirsis, G. Energy management and storage systems on electric vehicles: A comprehensive review. *Mater. Today Proc.* **2022**, *61*, 813–819. [[CrossRef](#)]
21. Tie, S.F.; Tan, C.W. A review of energy sources and energy management system in electric vehicles. *Renew. Sustain. Energy Rev.* **2013**, *20*, 82–102. [[CrossRef](#)]
22. Google Maps. Available online: <https://maps.google.com> (accessed on 23 March 2024).
23. Geo Tracker. Available online: <https://geo-tracker.org/en> (accessed on 23 March 2024).
24. Petal Maps. Available online: <https://www.petalmaps.com> (accessed on 23 March 2024).
25. Sygic. Available online: <https://www.sygic.com> (accessed on 23 March 2024).
26. Waze. Available online: <https://www.waze.com> (accessed on 23 March 2024).
27. Role of Car Batteries in Hybrid Vehicles. CarBike360. Available online: <https://www.carbike360.ae/articles/car-batteries-in-hybrid-vehicles> (accessed on 5 April 2024).
28. Automotive Electronics. Electric Vehicles and Hybrid Power Systems. EV Battery Management System (BMS). MPS. Available online: [https://www.monolithicpower.com/en/automotive-electronics/electric-vehicles-and-hybrid-power-systems/ev-battery-management-systems#:~:text=Electric%20vehicles%20\(Evs\)%20and%20hybrid,%20dependability,%20and%20peak%20performance](https://www.monolithicpower.com/en/automotive-electronics/electric-vehicles-and-hybrid-power-systems/ev-battery-management-systems#:~:text=Electric%20vehicles%20(Evs)%20and%20hybrid,%20dependability,%20and%20peak%20performance) (accessed on 5 April 2024).
29. Toyota Hybrid—How Does It Works? Joe Clifford. Posted on 9 July 2020. Available online: <https://mag.toyota.co.uk/how-does-toyota-hybrid-work/> (accessed on 5 April 2024).
30. Hyundai. Features. Energy Flow. Available online: <https://www.hyundai.com/eu/models/tucson-plug-in-hybrid/features.html> (accessed on 5 April 2024).
31. How Do the Electric Engines and Combustion Engine Work Together? How a Full Hybrid Works. Renault. Available online: <https://www.renault.co.uk/engines-innovation/help-use-hybrid.html> (accessed on 5 April 2024).
32. What Is an EV Battery State of Charge (SOC). EV Engineering. Aharon Etengoff. Posted on 13 December 2023. Available online: <https://www.evengineeringonline.com/what-is-an-ev-battery-state-of-charge-soc/#:~:text=Maximizing%20performance:%20EV%20batteries%20deliver,%25%20to%2080%25%20SOC%20range> (accessed on 5 April 2024).
33. Hofman, T.; Dai, C.H. Energy Efficiency Analysis and Comparison of Transmission Technologies for an Electric Vehicle. Technische Universiteit Eindhoven (TU/e) Department of Mechanical Engineering, Control Systems Technology Group, Eindhoven, The Netherlands. 2010. Available online: <https://www.iri.upc.edu/people/riera/VPPC10/vppc2010.univ-lille1.fr/uploads/PDF/papers/RT4/95-43218-final.pdf> (accessed on 7 April 2024).
34. Armenta-Déu, C.; Boucheix, B. Evaluation of Lithium-Ion Battery Performance under variable climatic conditions: Influence on the Driving Range of Electric Vehicles. *Future Transp.* **2023**, *3*, 535–551. [[CrossRef](#)]
35. Armenta-Déu, C. *Analysis of the Performance of a Light-Duty Hybrid Electric Vehicle for Daily Urban Route under Standard Traffic Conditions*; Internal report CAD-RC/e-tech 01/24; UCM: Madrid, Spain, 2024.
36. Speed Limit by Country. Speed Limits by Country—Wikipedia. Available online: https://en.wikipedia.org/wiki/Speed_limits_by_country (accessed on 8 April 2024).

37. Worldwide Daily Driving Distance. Available online: <https://www.solaronev.com/post/average-daily-driving-distance-for-passenger-vehicles#:~:text=While%20the%20EU%20also%20shows,most%20at%2037.7km%20daily> (accessed on 4 April 2024).
38. Armenta-Déu, C.; Rincón, C.; Pedrosa, S. Analysis of Driving patterns in Urban Zones. Project RUTW-CAM56: Sustainable Urban Transportation in Cities. Report 01/24. 2024. Available online: <https://www.google.com.hk/url?sa=t&source=web&rct=j&opi=89978449&url=https://www.preprints.org/manuscript/202404.0747/v1/download&ved=2ahUKEwjwqqiHsLeGAxV5hLYBHX9HKOwQFnoECA4QAQ&usg=AOvVaw2RLim4miSgNm-uuJK1LL6O> (accessed on 8 April 2024).

Disclaimer/Publisher's Note: The statements, opinions and data contained in all publications are solely those of the individual author(s) and contributor(s) and not of MDPI and/or the editor(s). MDPI and/or the editor(s) disclaim responsibility for any injury to people or property resulting from any ideas, methods, instructions or products referred to in the content.